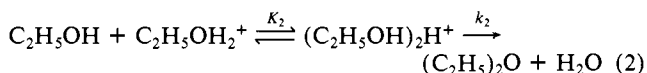
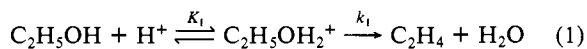


Figure 1. Rates of the formation of diethyl ether and ethylene from ethanol over $\text{H}_3\text{PW}_{12}\text{O}_{40}$ (ethanol basis) as well as the amount of absorbed ethanol under the working conditions as a function of the partial pressure of ethanol. Reaction temperature: 130 °C, W/F (ratio of the catalyst weight to the feed rate): 2–60 $\text{g}\cdot\text{h}\cdot\text{mol}^{-1}$.

Figure 1 shows the pressure dependencies of the rates of ether and ethylene formation observed for $\text{H}_3\text{PW}_{12}\text{O}_{40}$. The rates increased at first with increasing ethanol pressure (ca. 0.5–0.8th order) but then decreased markedly at higher pressures with the maximum clearly occurring at a higher pressure for the formation of ether. This pressure dependency is quite different from those observed for ordinary solid acids like $\text{SiO}_2\text{-Al}_2\text{O}_3$ and Al_2O_3 ; on such solid acids the formation of ethylene is usually zero order and that of ether zero to first order.⁶ Moreover, the catalytic activity of $\text{H}_3\text{PW}_{12}\text{O}_{40}$ was 10^2 times greater than $\text{SiO}_2\text{-Al}_2\text{O}_3$.

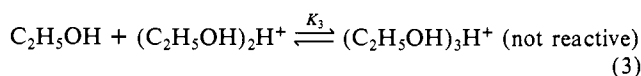
The amounts of absorbed ethanol were determined as shown in Figure 1. The amount increased from 0.4 to 8 molecules/anion as the partial pressure of ethanol increased from 0.4 to 60 kPa. These amounts correspond to 4–80 times the monolayer (ca. 20–400 times the number of the surface polyanions), showing that most of the ethanol molecules were absorbed into the bulk. Therefore, it is very likely that the ethanol reaction proceeds mainly in the absorbed phase, just as we showed for dehydration of 2-propanol.³

It is also worth noting that the amount of absorbed ethanol varied, apparently corresponding to the changes in the rates. Since ethylene is formed from one molecule of ethanol and ether from two molecules, ethylene may be preferably formed when the ratio of ethanol to protons in the pseudoliquid phase is low, and ether may be favored as the ratio increases. Equations 1 and 2 present a reasonable mechanism. Reactions similar to the first parts of



eq 1 and 2 occur for pyridine absorbed into a $\text{H}_3\text{PW}_{12}\text{O}_{40}$ lattice: $\text{py} + \text{H}^+ \rightleftharpoons \text{H}^+\text{py}$ and $\text{py} + \text{H}^+\text{py} \rightleftharpoons (\text{py})_2\text{H}^+$.⁷ Since, in the present case, the amount of absorbed ethanol increased sharply at about 15 kPa and was accompanied by a rapid decrease of the

reaction rate, a phase change at this pressure to an inactive phase containing too much ethanol is indicated. In other words, $(\text{C}_2\text{H}_5\text{OH})_n\text{H}^+$ ($n \geq 3$) is much less reactive for the formation of both products.



According to this model, the concentrations of monomer ($\text{C}_2\text{H}_5\text{OH}_2^+$), dimer ($(\text{C}_2\text{H}_5\text{OH})_2\text{H}^+$), and oligomer increase in first, second, and higher order, respectively, with respect to the ethanol pressure. So this model explains the essential trends found in Figure 1, for example, the maximum rate of ether formation was at a higher partial pressure of ethanol than that for ethylene formation, and the rates for both reactions were low at high ethanol pressures. For example, with K_1 , K_2 , and K_3 values of 2.3×10^{-4} , 5.3×10^{-4} , and $7.5 \times 10^{-6} \text{ Pa}^{-1}$, respectively, the general trends were fairly well reproduced. Since the absorption-desorption processes are rapid, it is not rate-controlling step. Hence the dehydration can take place homogeneously in the bulk phase. This is the pseudoliquid phase which provides a unique reaction media for organic reactions and also makes spectroscopic studies of catalytic processes very feasible.^{7,8}

Further evidence for the pseudoliquid phase is provided by examining $\text{Cs}_3\text{PW}_{12}\text{O}_{40}$. In the case of the Cs salt, only ether was formed on a zero-order reaction. The amount of ethanol absorbed was ca. 0.5 molecules/anion (0.4 times the monolayer) and nearly constant over the pressure range. This behavior corresponds closely to that observed for ordinary solid acids in the limiting case of high partial pressure.⁶ The difference between the acid form and the Cs salt is explained by the very different absorptivity of these compounds,⁴ and the Cs salt shows no tendency to exhibit a pseudoliquid phase.

(8) Highfield, J. G.; Moffat, J. B. *J. Catal.* **1986**, *98*, 245–258.

Carboxypeptidase A: Novel Enzyme-Substrate-Product Complex

David W. Christianson[†] and William N. Lipscomb*

Gibbs Chemical Laboratories
Department of Chemistry, Harvard University
Cambridge, Massachusetts 02138

Received April 20, 1987

As part of our continuing X-ray crystallographic studies of carboxypeptidase A (CPA) and its interaction with inhibitors^{1–6} and substrates,⁷ we now report the structure of the complex between CPA and the slowly hydrolyzed substrate *N*-benzoyl-L-phenylalanine (BZF).^{8,9} More properly, the structure observed at room temperature as well as slightly subzero temperature is that of an enzyme-substrate-product complex. The structure also represents an enzyme-products complex for the hydrolysis of *N*-benzoyl-L-phenylalanine-L-phenylalanine and may depict the

[†] AT&T Bell Laboratories Scholar.

(1) Christianson, D. W.; Lipscomb, W. N. *Proc. Natl. Acad. Sci. U.S.A.* **1985**, *82*, 6840–6844.

(2) Christianson, D. W.; Kuo, L. C.; Lipscomb, W. N. *J. Am. Chem. Soc.* **1985**, *107*, 8281–8283.

(3) Christianson, D. W.; Lipscomb, W. N. *J. Am. Chem. Soc.* **1986**, *108*, 545–546.

(4) Christianson, D. W.; Lipscomb, W. N. *J. Am. Chem. Soc.* **1986**, *108*, 4998–5003.

(5) Christianson, D. W.; Lipscomb, W. N. In *Zinc Enzymes*; Bertini, I., Luchinat, C., Maret, W., Zeppezauer, M., Eds.; Birkhauser: Boston, 1986; pp 121–132.

(6) Christianson, D. W.; David, P. R.; Lipscomb, W. N. *Proc. Natl. Acad. Sci. U.S.A.* **1987**, *84*, 1512–1515.

(7) Christianson, D. W.; Lipscomb, W. N. *Proc. Natl. Acad. Sci. U.S.A.* **1986**, *83*, 7658–7672.

(8) Hofmann, K.; Bergmann, M. *J. Biol. Chem.* **1940**, *132*, 225–235.

(9) Grobely, D.; Goli, U. B.; Galardy, R. E. *Biochemistry* **1985**, *24*, 7612–7617.

(6) Knözinger, H. *Angew. Chem., Int. Ed. Engl.* **1968**, *7*, 791–805. Figueras Roca, F.; De Mourgues, L.; Trambouze, Y. *J. Catal.* **1969**, *14*, 107–113. de Boer, J. H.; Fahim, R. B.; Linsen, B. G.; Vissere, W. J.; de Vleeschauer, W. F. N. M. *J. Catal.* **1967**, *7*, 163–172.

(7) Misono, M.; Mizuno, N.; Katamura, K.; Kasai, A.; Sakata, K.; Okuhara, T.; Yoneda, Y. *Bull. Chem. Soc. Jpn.* **1982**, *55*, 400–406.

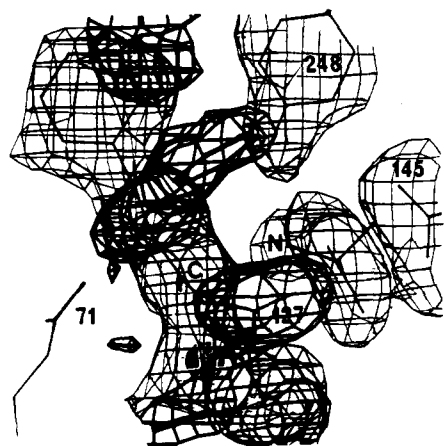


Figure 1. Difference electron density map calculated with Fourier coefficients $5|F_o| - 4|F_c|$ and phases calculated from the refined model omitting active site arginines, Tyr-248, product phenylalanine, and intact BZF. Enzyme residues Arg-71, Arg-127, Arg-145, and Tyr-248 are indicated by their sequence numbers. The planar benzamido moiety of BZF is coming toward the viewer above and to the left of center; its amide carbonyl receives a hydrogen bond from Arg-71. The benzyl side chain of BZF occupies the upper left corner. Note the break in electron density between the BZF carboxylate ("C") and the amino nitrogen ("N") of cleaved phenylalanine. Arg-127 has moved closer to the zinc environment in order to accommodate the binding of the BZF carboxylate.

"Michaelis complex" for the reverse, synthetic reaction. Interestingly, synthetic reactions have been exploited by Breslow and Wernick^{10,11} and more recently by Geoghegan and colleagues¹² in mechanistic studies of CPA.

Crystals of CPA were prepared and cross-linked as described¹ and then soaked in a buffer solution [0.15 M LiCl, 0.02 M Veronal-LiOH (pH 7.4)] containing 0.1 M BZF for 3 days at room temperature. X-ray data were collected from these crystals to a limiting resolution of 1.8 Å. Typical procedures and calculations have been described.¹ Model building was performed on an Evans and Sutherland PS300 by using the graphics program FRODO.¹³ The crystallographic *R* factor¹⁴ for the final model is 0.187 at 1.8-Å resolution.

The structure of the ternary complex reveals one molecule of phenylalanine, cleaved from BZF, in the S_1' hydrophobic pocket—its carboxylate is salt linked to Arg-145. This carboxylate also receives hydrogen bonds from Asn-144 and Tyr-248. An intact BZF molecule occupies the S_1 and S_2 subsites; its carboxylate is asymmetrically coordinated to zinc, with Zn–O distances¹⁵ of 2.7 and 2.2 Å. The latter oxygen is also 3.3 Å from Arg-127; within experimental error¹⁵ this distance corresponds to a hydrogen bond. A clean break in electron density (Figure 1) separates the intact BZF molecule from product phenylalanine, and the carboxylate carbon of BZF is 3.3 Å from the amino group of phenylalanine. The BZF carboxylate is rather close to the γ -carboxylate of Glu-270 (the closest oxygen–oxygen contact is 2.5 Å), so either carboxylate may be protonated in order to avoid an electrostatically unfavorable interaction. If the BZF carboxylate is protonated, the observed complex may be productive for synthesis. The amino nitrogen of phenylalanine is in proper orientation for attack by its lone pair at the π^* orbital of a BZF carboxylic acid.

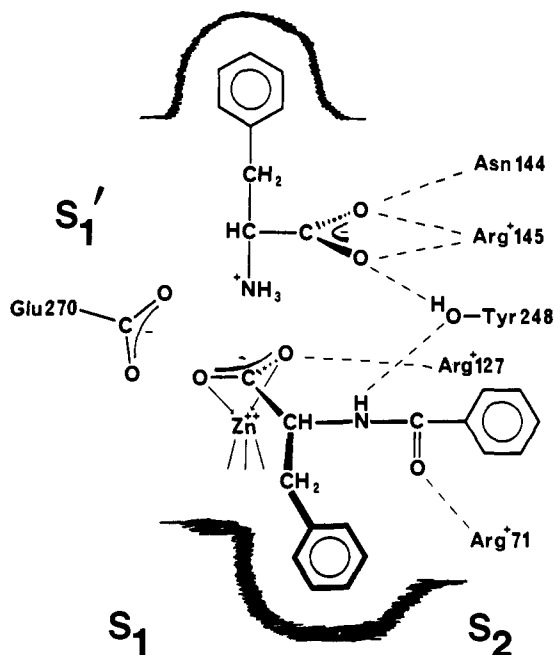


Figure 2. Schematic illustration of the ternary CPA–BZF–phenylalanine complex. Subsites on the enzyme are designated by the conventional notation as S_1' , S_1 , and S_2 . This binding mode provides a previously unconsidered model for substrate inhibition and highlights a hydrophobic cleft in the S_1 subsite on the enzyme. It also represents a products complex for the hydrolysis of *N*-benzoyl-L-phenylalanine-L-phenylalanine. As such, it shows for the first time that a product carboxylate can bridge the zinc ion and Arg-127. Both the zinc ion and Arg-127 may serve to polarize the carboxylic acid as the first step of the reverse, synthetic reaction.

The benzyl group of intact BZF lies in the aromatic cleft of the S_1 subsite which is defined by enzyme residues Tyr-198, Ser-199, Leu-201, Ile-247, and Tyr-248. This cleft contributes to the enzyme's preference for substrates with aromatic P_1 side chains.¹⁶ The phenyl group of the BZF side chain is in a favorable "edge-to-face" orientation with Tyr-198. Likewise, the phenyl group of the *N*-terminal benzoyl moiety tends toward a similar interaction with Tyr-248. Interactions of this type have been recently discussed¹⁷ and may be important for the interaction of enzymes with certain substrates. The amide carbonyl of the intact BZF molecule is hydrogen bonded to Arg-71 (2.9 Å), and the amide NH donates a hydrogen bond to Tyr-248 (3.1 Å). These hydrogen bonds were also observed in the complex with the cleaved inhibitor from the potato.¹⁸ However, the product carboxylate in this study¹⁸ was observed to bridge the zinc ion and Tyr-248. Nevertheless, the ternary complex of the present study shows that Arg-127 can bind the product carboxylate of amino acids occupying the S_1 subsite (Figure 2).

The current structure reveals a mode of substrate inhibition previously unconsidered for CPA. The hydrophobic cleft of the S_1 subsite is expected to facilitate this binding mode for substrates which have bulky aromatic side chains. It must be stressed that the intact BZF is not bound productively—its scissile amide carbonyl is too far away from the catalytic elements (Glu-270, the zinc ion, and Arg-127) of the active site.^{4,6,7} Although Vallee and colleagues propose a productive binding mode for esters involving the coordination of the terminal carboxylate to zinc,¹⁹ the location of BZF as observed here cannot represent such a binding mode. Furthermore, our attempts to model an ester positioned in the S_1' subsite with its carboxylate coordinated to zinc tend to move the ester out of the hydrophobic pocket. Therefore, we maintain that differences between esterolysis and

(10) Breslow, R.; Wernick, D. *Proc. Natl. Acad. Sci. U.S.A.* **1977**, *74*, 1303–1307.

(11) Breslow, R.; Wernick, D. *J. Am. Chem. Soc.* **1976**, *98*, 259–261.

(12) Geoghegan, K. F.; Galdes, A.; Hanson, G.; Holmquist, B.; Auld, D. S.; Vallee, B. L. *Biochemistry* **1986**, *25*, 4669–4674.

(13) Jones, T. A. In *Computational Crystallography*; Sayre, D., Ed.; Clarendon: Oxford, 1982; pp 303–317.

(14) $R = \frac{\sum ||F_o| - |F_c||}{\sum |F_o|}$, where $|F_o|$ and $|F_c|$ are observed and calculated structure factor amplitudes, respectively.

(15) An estimate of the upper limit in the rms error of atomic positions is about 0.2 Å based upon relationships derived by Luzzati, see: Luzzati, V. *Acta Crystallogr.* **1952**, *5*, 802–810.

(16) Smith, E. L. *J. Biol. Chem.* **1948**, *175*, 39–47.

(17) Burley, S. K.; Petsko, G. A. *J. Am. Chem. Soc.* **1986**, *108*, 7995–8001.

(18) Rees, D. C.; Lipscomb, W. N. *J. Mol. Biol.* **1982**, *160*, 475–498.

(19) Vallee, B. L.; Galdes, A.; Auld, D. S.; Riordan, J. F. In *Metals Ions in Biology*; Spiro, T. G., Ed.; Wiley: New York, 1983; Vol. 5, pp 25–75.

